A Harmonious Image Analysis Workflow for Large Format Electron Microscopy: Web-Based Collaboration and Local Processing Enabling Rigorous GABA-Post-Embedding Immunogold Quantification

C. Clarkson-Paredes[1], C.A. Brantner[1], C. Zugates[2], M. Rust[3], *A.S. Poptratiloff[1]

[1]Nanofabrication and Imaging Center (GWNIC), The George Washington University, Washington, DC; [2]arivis Inc, Washington, DC; [3]arivis AG, Rostock, Germany

THE GEORGE WASHINGTON UNIVERSITY · WASHINGTON, DC

arivis

Introduction

Biological electron microscopy (EM) image segmentation and analysis is complicated due to a huge complexity of shapes and intensities presented at single biological data sets. Thus many of the classical image analysis approaches relaying on intensity threshold, spatial filtering and object separation cannot be easily employed for object segmentation in EM data sets. Machine learning approaches are promising venue, but processing power, readily accessible algorithms and outcome quality assurance will present barriers for routine application for years to come. In neurosciences, high quality, large EM data sets can be generated by many scanning electron microscopes (SEM) using low landing voltage electrons and using elastically backscattered detection. Such images present the structural information of the same quality as transmission electron microscopy data, but with naturally inverted intensity.

Previously, large scale analysis of changes in the amount and localization of molecules in the brain using post-embedding immunogold labeling was near to impossible due to spatial constrains of TEM-sample holders. We have devised an approach enabling us to produce very large area high-resolution SEM images, in a scale of quality and resolution comparable to the biological TEM. With this approach we investigate alterations of the inhibitory neurotransmission (γ-aminobutyric acid-GABA) in the hypoglossal nucleus (XIIN) of LgDel mice, - an accurate animal model of 22q11.2 deletion syndrome. Defects of GABA-ergic neurotransmission have been postulated to be the foundation of altered neuronal synchrony (Sigurdsson et al., 2010), while in LgDel mice a significant reduction of GABA-ergic IPSC frequency but not amplitude in hypoglossal motor neuron was documented (Wang et al., 2017). To further investigate GABA alterations in the hypoglossal nucleus, in particular in the synaptic terminals we devised an approach that combines large ultra-thin sections (120 nm) containing the entire brainstem of a mouse with post-embedding immunogold detection of GABA (Fig. 1). This multi-layered image acquisition approach provides a solid framework to collect high resolution data based on lower resolution structural context data. In addition, we devised a logical pipeline based on arivs WebView and arivis Vision4D to segment and quantify gold particles encoding GABA inside the synaptic terminals. (Fig. 2 and 3).
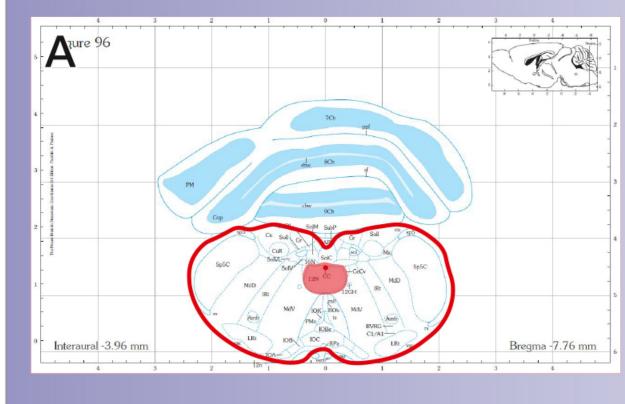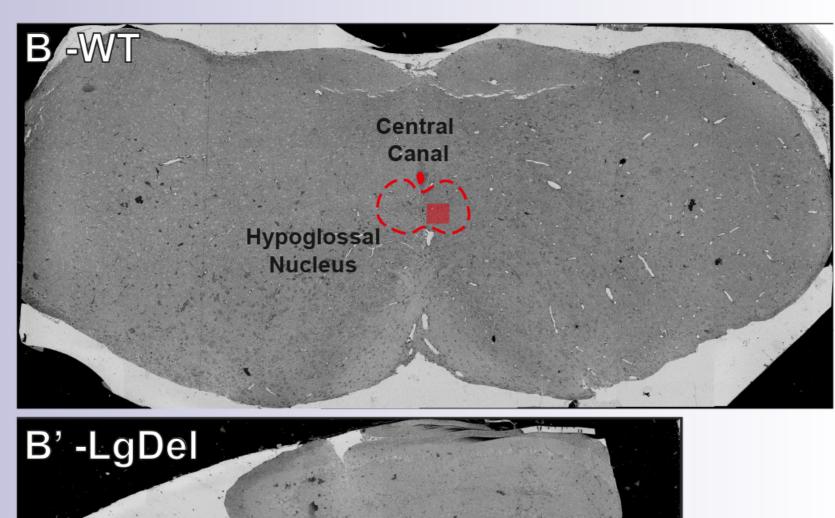

Fig 1. Hypoglossal nucleus location in the mouse brainstem on epoxy embedding resin. (A) Coronal IA level showing the location of hypoglossal nucleus. (B and B') Stitched low magnification (650x/SFV) overviews of a brainstem section for WT (B) and LgDel (B') animal stained against GABA showing the hypoglossal nucleus location. Highlighted in red the acquisition site per animal.

Material & Methods

The sections were first mounted on silicon wafers and then processed for post-embedding immunogold following conventional protocol. We pre-treated the sections for epoxy resin etching with 1% sodium metaperiodate by 20 min, then sections were pre-blocked with 1% NGS for 10 min and then incubated with a rabbit anti-GABA (A2052 Sigma-Aldrich) in TBST containing 1% NGS for 3 hr. at 37°C. The primary antibody was recognized with a goat anti-Rabbit IgG gold-conjugated, 10 nm diameter secondary antibody (15726-1 Ted Pella) in TBST containing 1% NGS and polyethylene glycol (5mg/ml) for 1 hour at 37°C. We utilized Helios NanoLab 660 SEM (Thermo Fisher, FEI) with concentric backscattering detector in immersion mode. Individual images were taken at HFV of 6.38um (3072x2048 px). Gold particles encoding GABA are readily distinguishable, and appear round. To increase the incidence of sampling GABA positive and negative synaptic terminals, we stitched large areas (119x102 um, 70645x60616 px) of the hypoglossal nucleus, producing massive data sets. Synaptic terminal segmentation was crowd-sourced using arivis WebView - a flexible and modular commercial platform with collaborative Web tools (Fig. 2), allowing 3 investigators to simultaneously segment synaptic terminals. We built a workflow to convert image data into a pyramidal redundancy-free format and transfer it to a Web server, perform collaborative segmentations, and use our Web-derived results directly in optimized particle-counting and distribution analysis. Data transfer, processing, and analysis are performed using the same data structure and software platform.

STEP 1 Segmentation of Presynaptic Terminals and Mitochondria — Web-hosted images and database, standard web-browser interface

STEP 2 Development of an optimized GABA-counting algorithm — Feature-rich, multithreaded, interactive image processing

STEP 3 Computation of terminal GABA-density, custom coloring, and examination of results — Local execution of algorithm and coloring via lightweight recipes
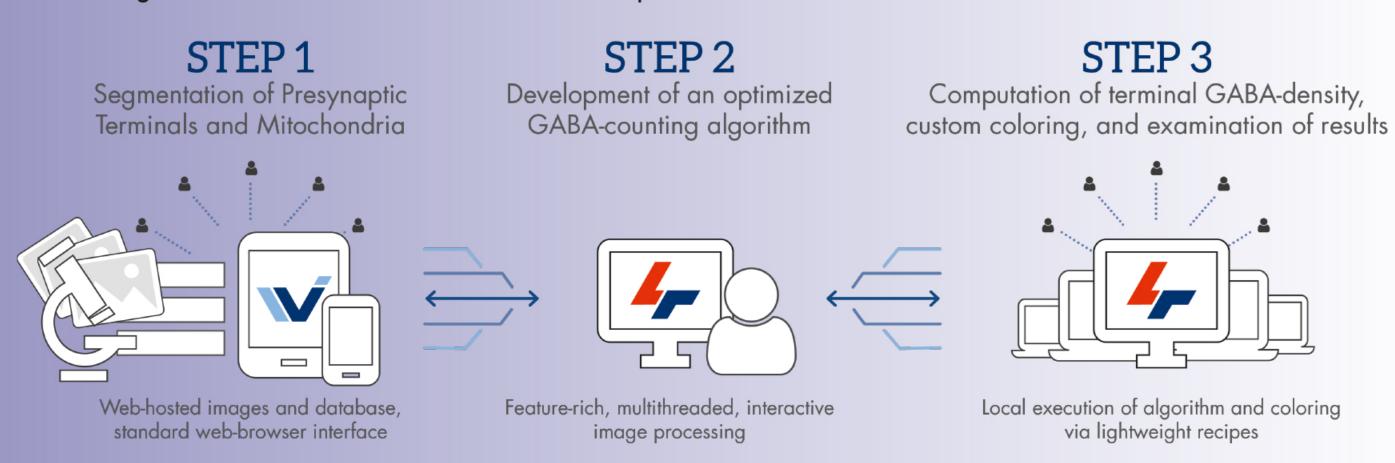
Fig 2. Overall scheme showing the workflow followed in the imaging segmentation and analysis using a commercial software.

To establish the thresholding between background staining and positive GABA synaptic terminals we used the Otsu method (Otsu, 1979), a non-parametric and unsupervised procedure of automatic threshold selection where an optimal threshold is selected by the discriminant criterion, not based on the differentiation, but on the integration of the histogram (Fig. 3).
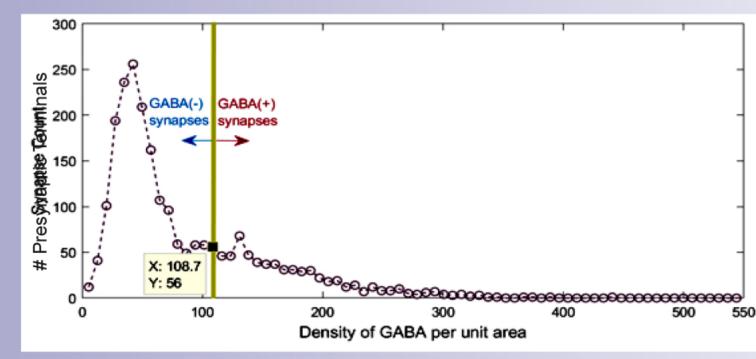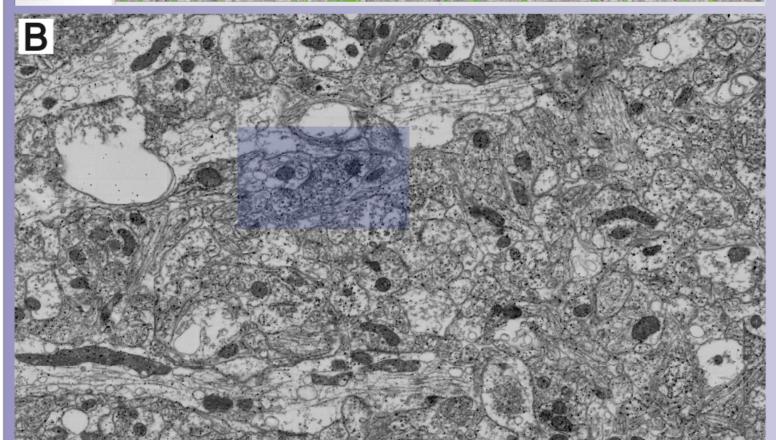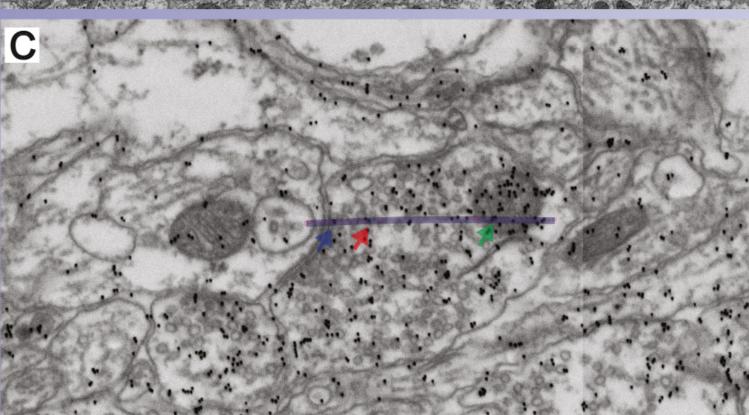

Fig 3. The Otsu method fixed the threshold for both groups (WT and LgDel) between background and "real" data in 108.7. Histogram showing the distribution of gold particles density for both groups analyzed.

Fig 4. Pipeline analysis for GABA immunogold labeling using arivis WebView and Vision4D
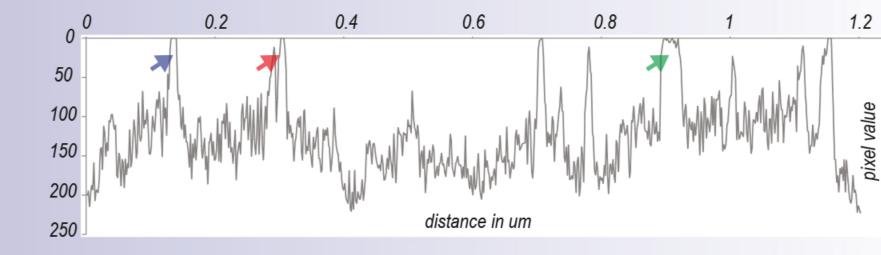

A: We converted the stitched *.RAW image data generated on FEI/Thermo Fisher Helios NanoLab 660 to the Scalable Image Storage (*.SIS) file format. This format enables instant access to any portion of an image, regardless of size. For development of the image processing algorithm, we were able to apply individual operations or an entire series of operations to any part of the image. As a first step, the images were uploaded on arivis WebView and made available for manual segmentation by multiple investigators. All synaptic boutons present within the large area of the hypoglossal nuclei were manually annotated disregarding their morphology (i.e., vesicle size, shape, active zone morphology); mitochondria within those annotations were also outlined as separate annotations. At the end of this step, the Web-hosted annotations (associated with the Web-hosted *.SIS data), were downloaded via web browser and associated with local *.SIS data sets.
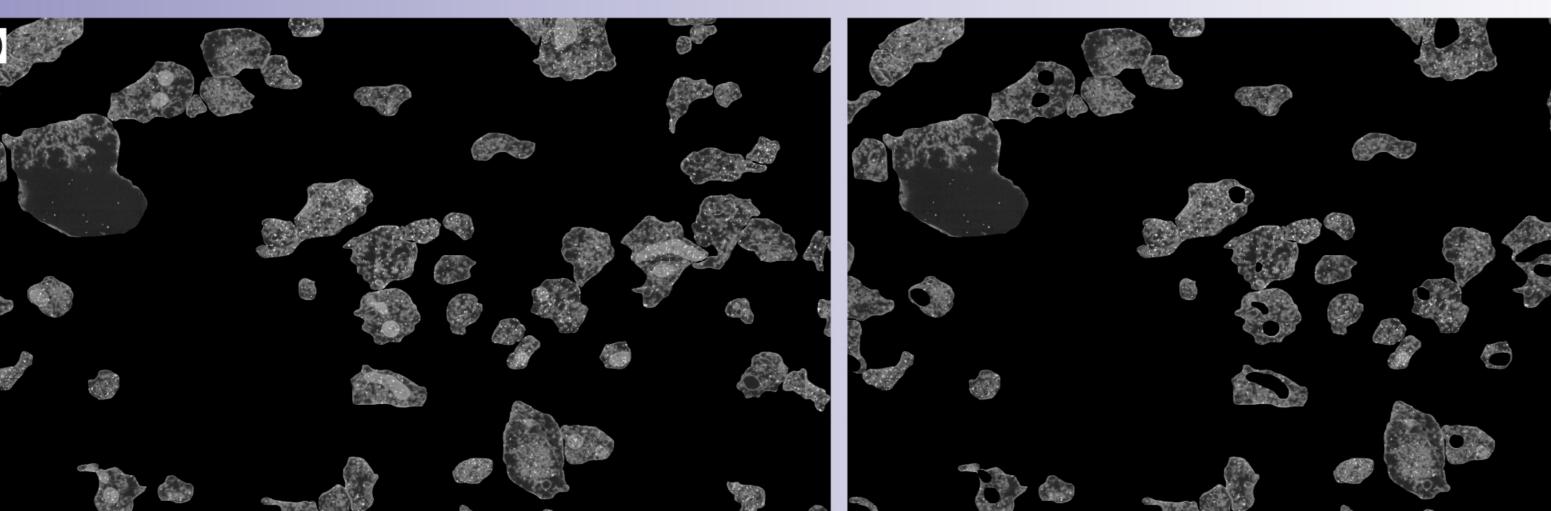
B: *.SIS image data sets were opened locally using arivis Vision 4D v3.0. We optimized the entire image processing algorithm for highest yield of reliable GABA-encoding gold particles detection. This panel shows the portion of the image that was selected to illustrate the processing that follows below. In general, using 2kV, 400pAmp landing electron beam and elastic scattering detection with concentric backscattering detector (CBS), allows for clear definition of the gold particles over the Uranium signal deriving from the counterstain. Although in principle the pixel brightness is somewhat proportional to the atomic composition of the sample probed by the pixel, two additional factors most likely contributed to the strong signal deriving from the lower atomic mass gold: 1*) the higher density of the gold particles relative to the sparser uranium, 2*) considerable gold particle-scattering detected in rings B-D. However, no topological information was detected with this imaging approach, indicating fewer if any secondary electron contribution to the signal.

C: Image depicting the boxed in region in B, showing two synaptic boutons establishing an active zone upon a dendrite. The purple line was used to generate a pixel intensity scan (graph below). Arrows indicate the signal deriving from each GP. Please note the intensity differential between the uranyl counterstain and the gold particle. The line scan plotted against pixel brightness, clearly illustrates that 1.6 nm pixel resolution is sufficient to resolve the signal registered from single gold particle (blue arrow) by applying single intensity threshold. This resolution is also supportive for intensity threshold separation of gold particles at a close proximity to each other (red arrow), but not sufficient to resolve clusters (green arrow). Therefore, we justified additional application of morphology filter in addition to the intensity threshold.

D: Although the signal from GABA-coding nanoparticles is naturally the strongest in the SEM images, for convenience of the investigators the luminosity was inverted in order to parallel the data achieved on TEM. However such an inversion is not entirely logical from the image processing perspective. Therefore as an initial step we applied an inverse filter, so that the gold particles present the brightest elements of the image data. This is followed by several processing steps in order to isolate the synaptic boutons from the rest of the image data set.
- Masking synaptic boutons (D left panel): The objects of the synaptic boutons that had been collaboratively segmented via the web were used to mask the image pixels so that only pixels corresponding to the interior of synaptic boutons are further processed in the subsequent steps.
- Inverse masking of mitochondria (D right panel): The GABA mitochondrial pool most likely represents GABA degradation rather than synaptic transmitter fraction. Therefore, the mitochondria objects that were collaboratively segmented via the web were used to inverse mask the image pixels that came from the synaptic boutons. This approach eliminates the pixels corresponding to mitochondria so that only pixels corresponding to synaptic boutons are processed by subsequent steps.

E: The next steps of the image processing were designed to isolate the signal from the gold particles encoding GABA and were performed in the following logical steps.
- Intensity thresholding to isolate GABA encoding gold particles signal (left). We found that the contrast highlighting GABA-coding gold particles (see above, C) was remarkably consistent throughout the entire large format images. Therefore a single global intensity threshold was capable to isolate the signal from the gold particles from the rest of the structural information. Pixels above the threshold value were passed to subsequent steps.
- Gaussian blur (not shown). In our preliminary algorithm optimization, we found that a subtle blur at this step increases the yield of truthful GABA dots and enhances the seed-based watershed segmentation later in the pipeline. This is well expected since the image data consist of variable white noise deriving from the gain applied to the detector and relatively short pixel integration times.
- Morphology to accentuate bright objects (middle). This morphology operation computes the difference between the input image and iterative erosion/dilation by a structuring element. Elements greater than the radius of the element passed this filter. This is a particularly effective strategy for extracting bright small details from an image, in this case the core of each GABA gold particle being represented by a small bright core. We found that in combination with the previous Gaussian blur we achieve a better yield of truthful dots.
- Seed-based Watershed (right). This final image processing step applies automatic seed-finding and a watershed segmentation. The operation uses the Gaussian scale to find the object seeds and a watershed algorithm to identify object boundaries. This step was necessary, since not all gold particles can be resolved by intensity threshold alone (see above, C green arrow). Once the gold particles are segmented, the objects could be further filtered to enrich for truthful pixels corresponding to gold particles and ultimately to associate gold particles with their parent synaptic boutons. All filters and associations are captured as tags in a relational database. Any feature or tag in this database can be used as a basis for sorting, for computation of custom object features, and can be visualized with colors and gradients.

F: The final product of the pipeline is an object database that maps to the original image pixel locations. Various morphometric parameters can be visualized at their original image location, while maintaining the relation of an object to the overall population. In this case (left), the original pixels were hidden and the image displays the terminal synaptic boutons (objects) with mitochondria excluded. The color is based on the terminal's concentration of GABA-encoding gold particles. Since the distribution is skewed, the red in the color table has also been skewed proportionally to reflect the fewer strongly labeled synaptic boutons.

Fig 5. Color coding- GABA terminal density distribution in the mouse hypoglossal nucleus. A (WT) and B (LgDel), high magnification (80,000x/SFV) tile stitched SEM images of the XIIN highlighted in Fig.1 showing color coding distribution of all synaptic terminals where 10 nm-gold particles were segmented. Notice the left shift to the blue (less dense) side in the LgDel animals, representing a decrease in the GABA content of presynaptic terminal in the XIIN versus WT animals.

Fig 6. Quantitative analysis of GABA content in presynaptic terminals from the hypoglossal nucleus of LgDel animals using post-embedding immunogold labeling and SEM. A) The number of GABA-GP significantly diminished in the LgDel animals while their distribution shifted to the left side showing the largest peak at 20 GP per terminal in comparison with the WT group where peak moves to 40 GP per terminal. B) Also, the presynaptic terminals area significantly decreased in LgDel group versus WT animals, supporting the idea of smaller terminals in LgDel model, the distribution of the areas in this model was higher for the smallest values, even when the number of terminals analyzed between groups (same area size) was similar. C) The density of GABA GP/distribution in the XIIN presynaptic terminals was lower in the LgDel group, which strongly indicates that the inhibitory neurotransmission of this nucleus in this animal model is altered due to a decrease in GABA content in presynaptic terminals. (****Mann-Whitney test- two tailed p<0.0001)